AD-A170 627 LABORATORY SIMULATION OF PLASMA STRUCTURE IN LATER-TIME HANE PLASMAS(U) JAYCOR SAN DIEGO CA J L SPERLING ET AL. 19 FEB 86 1/1

UNCLASSIFIED JAYCOR-J530-86-409/2448-00 DNA-TR-86-53 F/G 15/6 NL

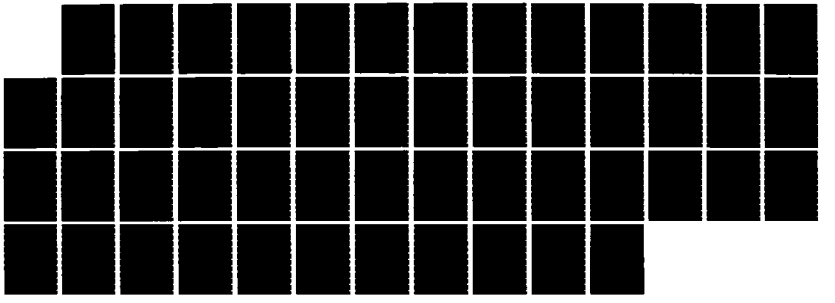

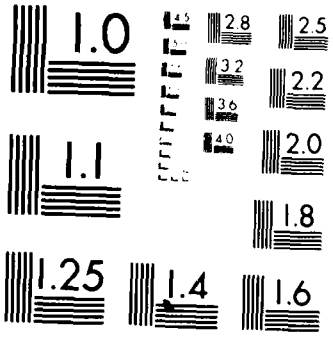

(12)

DNA-TR-86-53

LABORATORY SIMULATION OF PLASMA STRUCTURE IN LATER-TIME HANE PLASMAS

J. L. Sperling
P. G. Coakley
N. C. Wild
JAYCOR
P. O. Box 85154
San Diego, CA 92138-9259

19 February 1986

Technical Report

CONTRACT No. DNA 001-85-C-0345

THIS WORK WAS SPONSORED BY THE DEFENSE NUCLEAR AGENCY
UNDER RDT&E RMC CODE B310085466 RWRB 00006 25904D

Prepared for
Director
DEFENSE NUCLEAR AGENCY
Washington, DC 20305-1000

DISTRIBUTION LIST UPDATE

This mailer is provided to enable DNA to maintain current distribution lists for reports. We would appreciate your providing the requested information.

☐ Add the individual listed to your distribution list.

☐ Delete the cited organization/individual

☐ Change of address.

NAME: _____

ORGANIZATION: _____

OLD ADDRESS	CURRENT ADDRESS
_____	_____
_____	_____
_____	_____

TELEPHONE NUMBER: ( ) _____

SUBJECT AREA(s) OF INTEREST:

_____	_____
_____	_____
_____	_____

DNA OR OTHER GOVERNMENT CONTRACT NUMBER: _____

CERTIFICATION OF NEED-TO-KNOW BY GOVERNMENT SPONSOR (if other than DNA):

SPONSORING ORGANIZATION: _____

CONTRACTING OFFICER OR REPRESENTATIVE: _____

SIGNATURE: _____

UNCLASSIFIED
SECURITY CLASSIFICATION OF THIS PAGE

REPORT DOCUMENTATION PAGE

1a REPORT SECURITY CLASSIFICATION UNCLASSIFIED	1b RESTRICTIVE MARKINGS
2a SECURITY CLASSIFICATION AUTHORITY N/A since Unclassified	3 DISTRIBUTION/AVAILABILITY OF REPORT Approved for public release; distribution is unlimited.
2b DECLASSIFICATION/DOWNGRADING SCHEDULE N/A since Unclassified	
4 PERFORMING ORGANIZATION REPORT NUMBER(S) J530-86-409/2448-00	5. MONITORING ORGANIZATION REPORT NUMBER(S) DNA-TR-86-53
6a NAME OF PERFORMING ORGANIZATION JAYCOR 6b OFFICE SYMBOL (If applicable)	7a. NAME OF MONITORING ORGANIZATION Director Defense Nuclear Agency
6c. ADDRESS (City, State, and ZIP Code) P. O. Box 85154 San Diego, CA 92138-9259	7b. ADDRESS (City, State, and ZIP Code) Washington, DC 20305-1000
8a. NAME OF FUNDING/SPONSORING ORGANIZATION 8b OFFICE SYMBOL (If applicable)	9 PROCUREMENT INSTRUMENT IDENTIFICATION NUMBER DNA 001-85-C-0345
8c. ADDRESS (City, State, and ZIP Code)	10 SOURCE OF FUNDING NUMBERS PROGRAM ELEMENT NO: 62715H; PROJECT NO: RW; TASK NO: RB; WORK UNIT ACCESSION NO: DH009103

11 TITLE (Include Security Classification)
LABORATORY SIMULATION OF PLASMA STRUCTURE IN LATER-TIME HANE PLASMAS

12 PERSONAL AUTHOR(S)
Sperling, J. L.; Coakley, P. G.; and Wild, N. C.

13a TYPE OF REPORT	13b TIME COVERED	14 DATE OF REPORT (Year, Month, Day)	15 PAGE COUNT
Technical Report	FROM 850619 TO 860219	860219	50

16 SUPPLEMENTARY NOTATION
This work was sponsored by the Defense Nuclear Agency under RDT&E RMC Code B310085466 RWRB 00006 25904D.

17 COSATI CODES			18 SUBJECT TERMS (Continue on reverse if necessary and identify by block number)
FIELD	GROUP	SUB-GROUP	HANE, Power-Spectral Densities, Striations, Laboratory Simulations
20	9		
14	2		

19 ABSTRACT (Continue on reverse if necessary and identify by block number)

Because international treaties preclude high-altitude nuclear tests, there is little relevant experimental data from nuclear bursts regarding the size and dynamics of plasma structures or even the basic physical conditions permitting the evolution of plasma structures. JAYCOR has successfully demonstrated the feasibility of using its large plasma chamber to conduct an experimental study of the size and dynamics of striations in a controlled and highly diagnosed laboratory environment. The major accomplishments of the research have been (1) the development of scaling laws relating high-altitude nuclear and laboratory environments, (2) the determination of optimum experimental configurations for the laboratory simulations, (3) the development of adequate diagnostic techniques to evaluate the simulations, and (4) the development of a neutral-wind source.

20 DISTRIBUTION/AVAILABILITY OF ABSTRACT	21 ABSTRACT SECURITY CLASSIFICATION
☐ UNCLASSIFIED/UNLIMITED ☒ SAME AS RPT ☐ DTIC USERS	UNCLASSIFIED
22a NAME OF RESPONSIBLE INDIVIDUAL Betty L. Fox	22b TELEPHONE (Include Area Code) (202) 325-7042
	22c OFFICE SYMBOL DNA/STTI

DD FORM 1473, 84 MAR 83 APR edition may be used until exhausted
All other editions are obsolete

SECURITY CLASSIFICATION OF THIS PAGE
UNCLASSIFIED

CONVERSION TABLE

Conversion factors for U.S. Customary to metric (SI) units of measurement

MULTIPLY → / TO GET ←	BY → / BY ←	TO GET / DIVIDE
angstrom	1.000 000 X E -10	meters (m)
atmosphere (normal)	1 013 25 X E +2	kilo pascal (kPa)
bar	1 000 000 X E +2	kilo pascal (kPa)
barn	1.000 000 X E -28	meter^2 (m^2)
British thermal unit (thermochemical)	1.054 350 X E +3	joule (J)
calorie (thermochemical)	4 184 000	joule (J)
cal (thermochemical)/cm^2	4 184 000 X E -2	mega joule/m^2 (MJ/m^2)
curie	3 700 000 X E +1	*giga becquerel (GBq)
degree (angle)	1 745 329 X E -2	radian (rad)
degree Fahrenheit	$t_k = (t°f + 459\ 67)/1.8$	degree kelvin (K)
electron volt	1.602 19 X E -19	joule (J)
erg	1.000 000 X E -7	joule (J)
erg/second	1.000 000 X E -7	watt (W)
foot	3.048 000 X E -1	meter (m)
foot-pound-force	1.355 818	joule (J)
gallon (U S liquid)	3.785 412 X E -3	meter^3 (m^3)
inch	2 540 000 X E -2	meter (m)
jerk	1 000 000 X E +9	joule (J)
joule/kilogram (J/kg) (radiation dose absorbed)	1.000 000	Gray (Gy)
kilotons	4 183	terajoules
kip (1000 lbf)	4.448 222 X E +3	newton (N)
kip/inch^2 (ksi)	6 894 757 X E +3	kilo pascal (kPa)
ktap	1.000 000 X E +2	newton-second/m^2 ($N-s/m^2$)
micron	1 000 000 X E -6	meter (m)
mil	2.540 000 X E -5	meter (m)
mile (international)	1.609 344 X E +3	meter (m)
ounce	2.834 952 X E -2	kilogram (kg)
pound-force (lbs avoirdupois)	4.448 222	newton (N)
pound-force inch	1.129 848 X E -1	newton-meter (N·m)
pound-force/inch	1 751 268 X E +2	newton/meter (N/m)
pound-force/foot^2	4.788 026 X E -2	kilo pascal (kPa)
pound-force/inch^2 (psi)	6 894 757	kilo pascal (kPa)
pound-mass (lbm avoirdupois)	4 535 924 X E -1	kilogram (kg)
pound-mass-foot^2 (moment of inertia)	4 214 011 X E -2	kilogram-meter^2 ($kg \cdot m^2$)
pound-mass/foot^3	1 601 846 X E +1	kilogram/meter^3 (kg/m^3)
rad (radiation dose absorbed)	1 000 000 X E -2	**Gray (Gy)
roentgen	2 579 760 X E -4	coulomb/kilogram (C/kg)
shake	1 000 000 X E -8	second (s)
slug	1 459 390 X E +1	kilogram (kg)
torr (mm Hg, 0° C)	1 333 22 X E -1	kilo pascal (kPa)

*The becquerel (Bq) is the SI unit of radioactivity, 1 Bq = 1 event/s
**The Gray (Gy) is the SI unit of absorbed radiation

TABLE OF CONTENTS

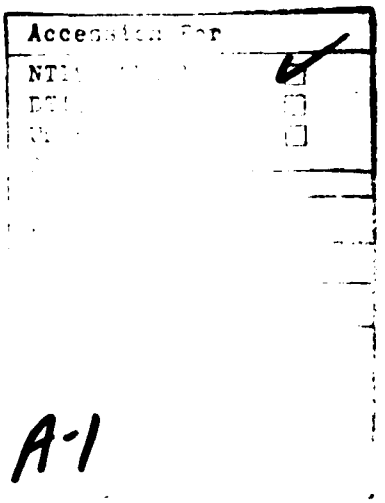

LIST OF ILLUSTRATIONS

SECTION 1
INTRODUCTION

Plasmas, in undisturbed or disturbed ionospheres and magnetospheres, can have an enormous range of parametric values. Accordingly, to understand the development of structures (e.g., striations) under all possible conditions, it is necessary to develop a formulation which includes a sufficient amount of physics to permit general applicability. Laboratory simulations of HANE environments can contribute substantially to the development of a complete phenomenological understanding of structure evolution in high-altitude nuclear plasmas as physical processes occur in a complete and natural way in the laboratory. Indeed, laboratory simulations could provide crucial and objective guidance in determining those physical effects which should be carefully considered in analytical and numerical models. By contrast, subjective decisions are often made in analytical and numerical studies in which plasma models are often predicated on simplicity or computational convenience.

As an example of how laboratory simulations may be used to improve analytical and numerical models, consider the possibility that laboratory simulations might demonstrate that kinetic effects (e.g., anomolous diffusion, drift waves, etc.) crucially affect structure evolution in some HANE environments. For such circumstances, the laboratory measurements could suggest effective kinetic transport coefficients for use in fluid simulations which cannot consider kinetic processes by themselves.

Furthermore, the laboratory simulations might demonstrate that finite temperature effects (e.g., temperature gradients and thermal conductivity) or the detailed dynamics of neutrals (e.g., neutral viscosity or the interaction of ions and electrons with neutrals) are important in some HANE environments and should be included in fluid simulations of later-time, high-altitude, nuclear, plasma structures. By contrast, present fluid simulations of later-time plasma structures generally do not include the contribution from plasma-temperature equations or equations describing neutral dynamics. Hence, laboratory simulations of HANE structure can have a very practical and crucial impact in the objective determination of the critical subset, within the complete set of plasma processes, which should be carefully considered in analytical and numerical models of the HANE environment.

Through their impact on the development of appropriate analytical or numerical models and through the data they provide, laboratory simulations of HANE plasma structures could provide the critical, but presently unavailable, experimental information for the development of accurate microstructure algorithms applicable to nuclear-effects simulations like SCENARIO.

The general objective of the research was to determine the feasibility of using a laboratory device to simulate later-time high-altitude, nuclear-structured plasmas. In this work, we developed scaling laws between HANE environments and the laboratory, and we determined optimum experimental configurations for the laboratory simulations. We also developed adequate diagnostic techniques to evaluate the simulations.

Scaling laws are derived for relating the evolution of plasma structures in the later-time HANE environment and the large plasma chamber at JAYCOR. Because the evolution of structure in later-time environments is expected to be well describable as an electrostatic and magnetostatic phenomenon, the proper scaling of the ion-gyroradius is argued to be extremely significant.[1] Indeed, theoretical analysis and more recent nonlinear, multidimensional computations clearly demonstrate the great significance of finite ion-gyroradius effects on striation "freezing".[2,3] To assure the proper scaling of the ion-gyroradius for reasonable magnetic-field strengths in the laboratory, we suggest that a fill gas with very low atomic mass (e.g., hydrogen) may be advantageously used in individual laboratory simulations.

The initial plasma configuration in the laboratory device and possible laboratory studies are described. For the cylindrical plasma chamber at JAYCOR a cylindrical density profile, with the electron density greater at smaller radii than at larger radii, is desirable and experimentally reasonable. The externally applied magnetic field is directed axially, and the externally-applied neutral wind is directed across the cylindrical plasma. With this plasma configuration, laboratory simulations can be undertaken for elucidating the role of parallel plasma currents and perpendicular plasma processes on the formation of striations. Experiments can also be conducted for determining the evolutionary characteristics of single striations and aggregates of striations.

The plasma diagnostics, for the laboratory simulation of structured plasmas in later-time HANE plasmas, are described as a variety of miniaturized particle collecting probes to measure plasma density, electron and ion temperatures, and electron density fluctuations.

Experiments have been successfully conducted to demonstrate the capability of two-probe correlation techniques to determine power-spectral densities in plasmas with density fluctuations.

The well-established technology of Laval nozzles is described as the means for obtaining the required neutral winds in the laboratory.

This report is divided into seven sections. Section 2 derives scaling laws relating the high-altitude nuclear environment and the laboratory tank at JAYCOR. Section 3 describes the initial plasma configuration in the laboratory device and possible laboratory studies. Section 4 describes the diagnostics, and Section 5 describes how two-probe correlation measurements can be used to determine power-spectral densities. Section 6 describes how a Laval nozzle can be used to obtain the required neutral winds. Section 7 is a summary and gives concluding remarks.

SECTION 2
SCALING LAWS

Scaling laws are derived for relating the evolution of plasma structures in the later-time HANE environment and the large plasma chamber at JAYCOR. Consideration is given to the possibility that the laboratory simulations may benefit from using matter different from that present in the HANE environment. Throughout, the symbol $\bar{}$ designates the ratio of laboratory to high-altitude nuclear quantities.

In the ionosphere the collisional drag between a neutral wind and ions is a significant driver in striation formation; consequently, it is desirable to preserve the ratio between mean free path and characteristic distance:

$$\bar{\rho} = \frac{\bar{A}}{\bar{\sigma}\,\bar{L}} \quad . \tag{1}$$

In Eq. (1) the following symbols are used: ρ (mass density), A (atomic mass), σ (binary collision cross section), and L (characteristic distance). Ion and neutral velocities are allowed to scale like the ion-thermal speed:

$$\bar{V} = \left(\frac{\bar{T}}{\bar{A}}\right)^{0.5} \quad , \tag{2}$$

with V (velocity) and T (temperature); therefore, a reasonable representation for the scaling of time (τ) is

$$\bar{\tau} = \frac{\bar{L}}{\bar{V}} = \bar{L}\left(\frac{\bar{A}}{\bar{T}}\right)^{0.5} \quad . \tag{3}$$

From Eqs. (1) and (3) it follows that the binary collision frequencies ($\bar{\nu}$) scale properly with time:

$$\bar{\nu} = \frac{\bar{\rho}}{\bar{A}}\,\bar{\sigma}\,\bar{V} = \frac{1}{\bar{\tau}} \quad . \tag{4}$$

Two different ways are considered for scaling the magnetic field (B). First, if the Alfven speed is preserved, then

$$\overline{B} = \overline{B}_A \equiv \overline{\rho}^{0.5} = \left(\frac{\overline{A}}{\overline{\sigma}\,\overline{L}}\right)^{0.5} \quad . \tag{5}$$

Second, if the ion-gyroradius is preserved, then

$$\overline{B} = \overline{B}_G \equiv \frac{\overline{V}\,\overline{A}}{\overline{Q}\,\overline{L}} = \frac{(\overline{T}\,\overline{A})^{0.5}}{\overline{Q}\,\overline{L}} \quad , \tag{6}$$

with $\overline{Q}$ being the scaling factor for charge state. The two different scalings for the magnetic field are completely consistent only if

$$1 = \frac{\overline{B}_A}{\overline{B}_G} = \overline{Q}\left(\frac{\overline{L}}{\overline{\sigma}\,\overline{T}}\right)^{0.5} \quad . \tag{7}$$

Equation (7) is independent of the scaling factor for atomic mass, $\overline{A}$. The discrepancy between Eqs. (5)-(6) also occurs in scaling studies between the early-time HANE environment and the laboratory.[1,4]

In the directions transverse to the magnetic field, striation evolution in the later-time HANE environment is expected to be an electrostatic and magnetostatic phenomenon.[5,6] Consequently, plasma dynamics associated with the propagation of Alfven waves across the magnetic field should have a corresponding negligible importance on the striation evolution. This contrasts with the much more rapid early-time evolution of the HANE environment when the geomagnetic field is strongly modified, and electromagnetic effects (e.g., Alfven waves) are important.[4]

Provided that all electric fields have a predominantly electrostatic character, Eq. (6) is easily shown to demonstrate proper scaling between Pedersen and parallel conductivities; therefore, there is proper scaling between perpendicular and parallel electric fields. However, with the use of Eq. (6), the propagation speed for Alfven waves along the magnetic field is much more rapid in the laboratory than if Eq. (5) is used instead to determine the magnetic-field strength. This means that parallel electric fields

correspondingly tend to be more electrostatic in the laboratory than in the high-altitude nuclear environment.[5,6] In this regard, theoretical studies at JAYCOR suggest that the formation of striations occurs for scale sizes transverse to the magnetic field which are sufficiently small so that parallel currents, whether inductive or electrostatic in character, are of secondary importance.[2,6]

In contrast to the Alfven speed, the finite size of ion gyroradii has been demonstrated to have a very strong effect on the linear evolution of collisional Rayleigh-Taylor instabilities;[2,3] moreover, the proper scaling of diffusion transverse to the magnetic field requires that the ion gyroradii, in addition to collision frequencies, scale correctly. The conclusion is that Eq. (6) is much better suited for scaling the magnetic field in the later-time HANE environment than Eq. (5).

Figure 1 is a summary of the basic scaling relations between striation phenomena in the later-time HANE environment and the laboratory.

Figures 2a and 2b are plots of $\bar{\rho}$, $\bar{A}/\bar{T}$, and $\bar{B}_G$ versus $\bar{L}$ for $\bar{T} = \bar{\sigma} = \bar{Q} = 1$. The scaling factor $\bar{B}_A$ is included in the figures for completeness. The difference between Figures 2a and 2b is that the gas used in the laboratory is assumed to be air ($\bar{A} = 1$) and hydrogen ($\bar{A} = 0.05$), respectively. For both Figures 2a and 2b, it is uniformly true that $\bar{B}_G > \bar{B}_A$; consequently, the constraint that the ion-gyroradius scale properly results in larger magnetic fields in the laboratory than would be necessary if the scaling of Alfven waves happened to be appropriate. The use of a gas with reduced atomic mass in the laboratory (i.e., $\bar{A} < 1$) does have the significant advantage of permitting reduced magnetic-field strengths in the laboratory consistent with the scaling laws.

As specific quantitative examples, consider a characteristic scale size of $\sim 10^4$ cm and ~ 1 cm for striations in the HANE environment and the laboratory, respectively; hence, $\bar{L} = 10^{-4}$. Figure 2a indicates that the mass density, evolution rate, and magnetic-field strength are 10^4 times larger in the laboratory than in the HANE environment. If the magnetic-field strength is 0.3 G in the HANE environment, then the scaling law for ion gyroradius suggests that the magnetic field be 3×10^3 G in the laboratory. Analogously from Figure 2b, $\bar{L} = 10^4$ implies that the mass density is 5×10^2 times larger in the laboratory than in the HANE environment. In the laboratory, the evolution rate and the magnetic-field strength are 4.5×10^4 and 2.2×10^3

mass density: $\bar{\rho} = \dfrac{\bar{A}}{\bar{\sigma}\,\bar{L}}$

velocity: $\bar{V} = \left(\dfrac{\bar{T}}{\bar{A}}\right)^{0.5}$

time: $\bar{\tau} = \bar{L}\left(\dfrac{\bar{A}}{\bar{T}}\right)^{0.5}$

magnetic field: $\bar{B} = \dfrac{(\bar{T}\,\bar{A})^{0.5}}{\bar{Q}\,\bar{L}}$

with

$\bar{A}$ = scaling factor for atomic mass

$\bar{\sigma}$ = scaling factor for collisional cross section

$\bar{L}$ = scaling factor for characteristic distance

$\bar{T}$ = scaling factor for temperature

$\bar{Q}$ = scaling factor for charge state

Figure 1. Basic scaling relationships for striation evolution in the later-time, high-altitude, nuclear environment and the laboratory.

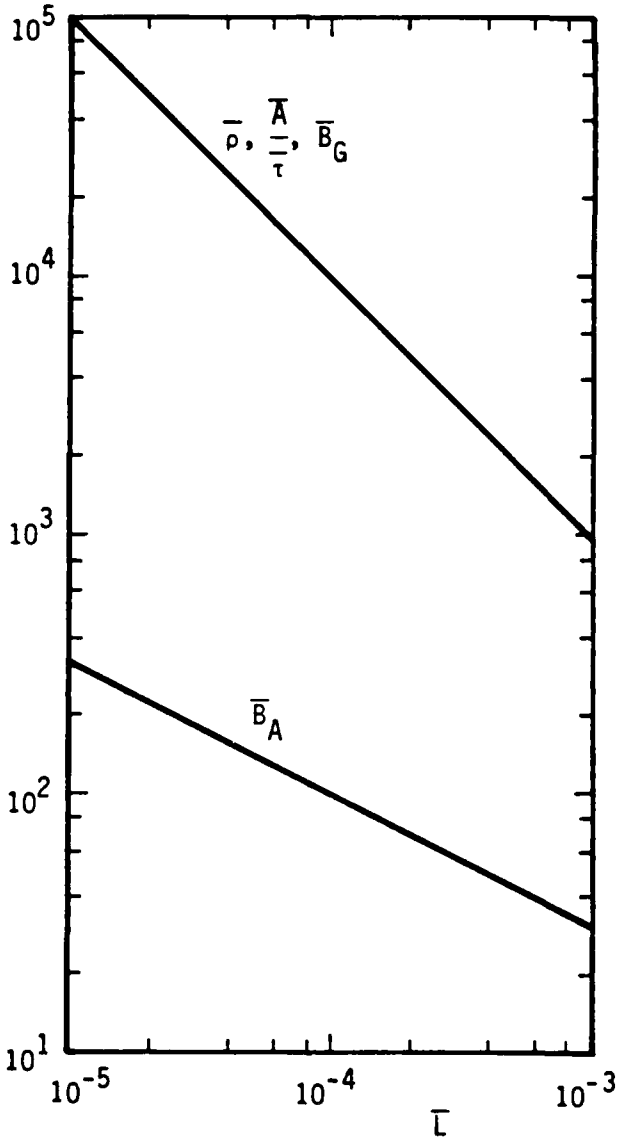

Figure 2a. $A/\bar{\tau}$, $\bar{\rho}$, $\bar{B}_G$, and $\bar{B}_A$ versus $\bar{L}$ for $\bar{T} = \bar{\sigma} = \bar{Q} = 1$ and $\bar{A} = 1$. $\bar{V} = 1$.

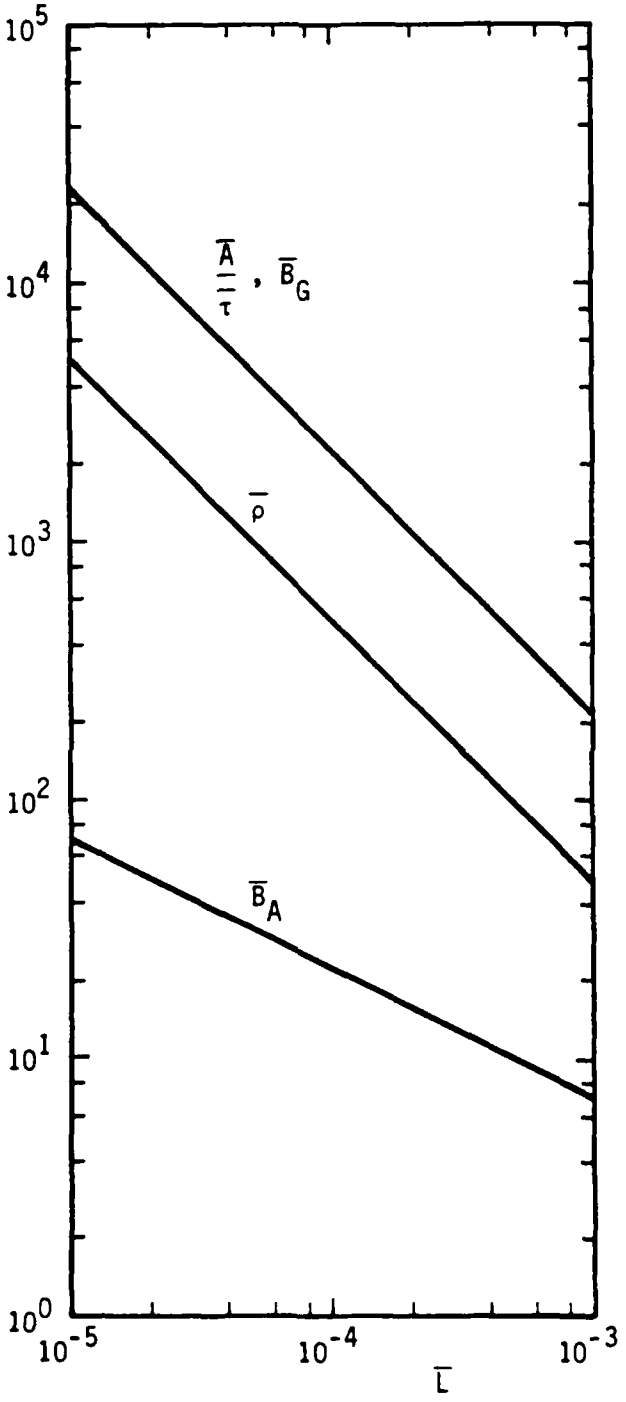

Figure 2b. $\overline{A}/\overline{\tau}$, $\overline{\rho}$, $\overline{B}_G$, and $\overline{B}_A$ versus $\overline{L}$ for $\overline{T} = \overline{\sigma} = \overline{Q} = 1$ and $\overline{A} = 0.05$. $\overline{V} = 4.47$.

times larger than in the HANE environment, respectively. For a magnetic-field strength of 0.3 G in the HANE environment, a magnetic-field strength of 6.6×10^2 G is implied in the laboratory.

Since magnetic field strengths $\lesssim 3 \times 10^3$ G should be attainable with the JAYCOR plasma chamber, air can be a realistic and reasonable material for at least some of the laboratory experiments. In addition, the use of a low atomic mass material like hydrogen should permit parametric studies over an especially large range of $\bar{L}$, the scaling factor for characteristic distance.

SECTION 3
INITIAL PLASMA CONFIGURATIONS AND LABORATORY STUDIES

The initial plasma configuration shown in Figure 3 appears reasonable for the laboratory simulation of structured plasmas in the later-time HANE environment. A cylindrical electron-density profile, n(r), is created in the JAYCOR plasma chamber tank with the electron density being greater at smaller radii than at larger radii. This density profile can be created by injection and subsequent rapid ionization of neutrals. The density profile does not need to be centered on the axis of the plasma chamber. The axial, z-directed, magnetic field with strength B confines electrons and ions. With a neutral wind, v_n, directed across the plasma, the density gradient and the neutral wind are antiparallel on the backside of the cylindrical plasma; consequently, the plasma becomes unstable to the Rayleigh-Taylor modes which are thought to be primarily responsible for the formation of striated plasmas in the HANE environment.

Even with the constraints imposed by the scaling laws described in Section 2, the basic plasma configuration has substantial flexibility to permit various types of relevant experiments. In the following paragraphs, the different types of experiments are synopsized through their division into three categories: (1) parallel plasma currents and the formation of striations, (2) perpendicular plasma processes and the formation of striations, and (3) evolution of single and aggregates of striations.

3.1 PARALLEL PLASMA CURRENTS AND THE FORMATION OF STRIATIONS.

References 6-8 provide clear quantitative demonstrations of how structures with large scale sizes across the magnetic field map greater distances along the magnetic field than structures with small transverse scale sizes. The key physical process is the short-circuiting of differences in the electrostatic potential between adjacent magnetic-field lines by the combination of finite parallel and finite perpendicular currents. The observation of sharp edges on ionospheric clouds transverse to the geomagnetic field[9-10] and additional theoretical evidence[2,6-8] suggests that whereas the evolution of large plasma clouds may strongly depend on parallel currents, the steep density gradients and the initial formation of Rayleigh-Taylor instabilities upon the steep density gradients are only weakly dependent upon parallel currents. Indeed, the suggestion has been made that an upper bound for the

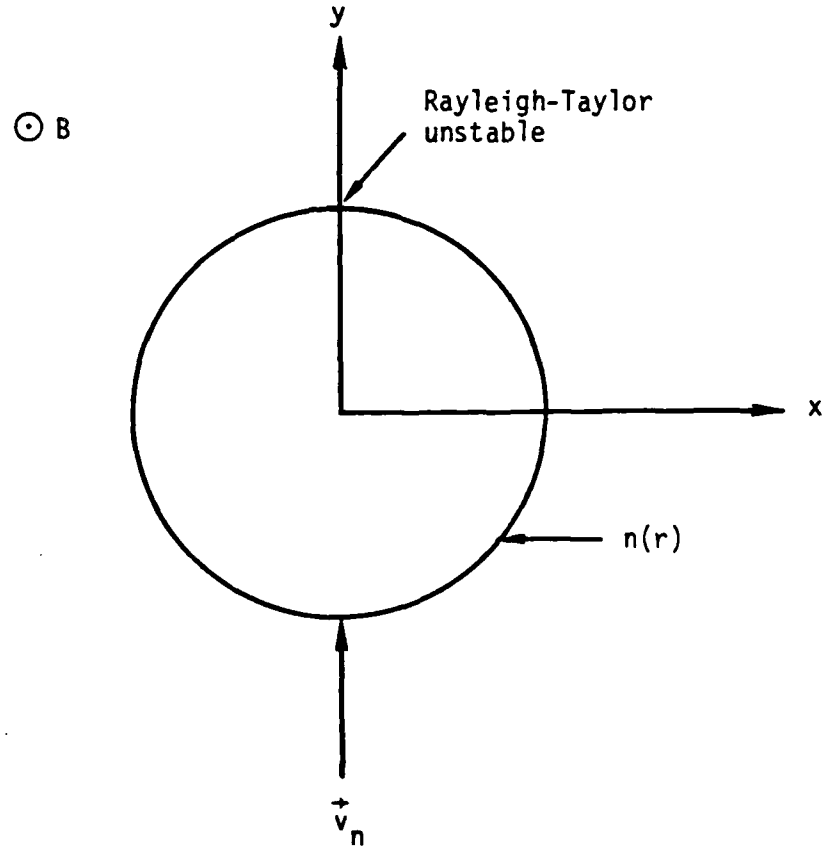

Figure 3. Initial plasma configuration for the laboratory simulation of structured plasmas in the later-time, high-altitude, nuclear environment.

scale size of striations transverse to the magnetic field is determined by the constraint that the contributions from parallel electron currents be negligible during the initial Rayleigh-Taylor evolution.[2]

The use of end plates with varying degrees of electrical insulation could be used to experimentally determine how parallel plasma currents impact the formation of sharp transverse density gradients and the subsequent formation of striations. With insulating end plates, parallel currents should be minimized; therefore, the transverse density gradients are predicted to have their largest possible value, and the maximum permissible transverse scale sizes for striations should increase.

At high-geomagnetic latitudes, particle precipitation and coupling between the ionosphere and the magnetosphere can substantially impact the development of plasma structures. With the capability for biasing the end plates in the laboratory tank at different voltages and the capability for injecting electron beams along the externally applied magnetic field, laboratory simulations of high-latitude plasma structures are possible. By biasing the end plates, experimental studies of how applied plasma currents affect the development of plasma structures can be conducted. Moreover, by injecting electron beams along the applied magnetic field, the effects of localized particle precipitation could be studied as a seed or as a direct source for plasma structures.

If the driving force transverse to the magnetic field (e.g., ion-neutral drag with a neutral wind) has finite extent along the magnetic-field direction as expected in the later-time HANE environment, the self-consistent current patterns are, in general, expected to have some finite components along the direction of the magnetic field. In the laboratory, the effects of finite parallel extent for driving forces can be simulated very simply by injecting the neutral wind across the magnetic field over a specified parallel distance. This would permit study of how the finite parallel extent of driving forces impacts the development of sharp transverse density gradients and the subsequent initial formation of striations.

3.2 PERPENDICULAR PLASMA PROCESSES AND THE FORMATION OF STRIATIONS.

Various theoretical and numerical studies have examined how plasma processes acting in the directions across the magnetic field affect the characteristics of striations, especially their transverse scale sizes.

Diffusion[9-11] and ion viscosity[2] are some of the more important plasma processes which have been considered.

As an example of how the laboratory simulations can be used to determine the dominant processes affecting the evolution of striations in the directions transverse to the magnetic field, consider the suggestion of Reference 2 that the lowest-order ion-gyroradius contributions to the ion-viscosity tensor are the major contributors to the observed scale sizes of striations transverse to the magnetic field. In particular, the theory of Reference 2 proposes the following expression for the tranverse wave number, k_t, characteristic of "frozen" striations:

$$k_t \sim \frac{1}{\rho_i}\left(\frac{\nu_{in}}{\Omega_i}\right)^{0.5} \quad . \tag{8}$$

In Eq. (8), the following symbols are used: ρ_i (ion-gyroradius), ν_{in} (ion-neutral collision frequency), and Ω_i (ion gyrofrequency). Figure 1 in Section 2 provides the relationship between parameters in the later-time HANE environment and the laboratory. The application of the scaling laws to Eq. (8) indicates that k_t scales properly as inverse distance; therefore, Eq. (8) not only gives a prediction for transverse striation scale sizes in the laboratory but it also predicts, in conjunction with the scaling laws, corresponding transverse striation scale sizes appropriate to the ionosphere. The observation that Eq (8) is satisfied in the laboratory would provide strong experimental evidence for its applicability in the later-time HANE environment within the ionosphere.

3.3 EVOLUTION OF SINGLE AND MULTIPLE STRIATIONS.

Figure 4 illustrates the qualitative evolution of striations as deduced from the observation of ionospheric barium clouds.[9] Similar evolution may be expected for HANE plasmas within the ionosphere. In particular, the initial evolution of linear Rayleigh-Taylor instabilities is soon followed by nonlinear development into sheets of ionization aligned along the direction of the magnetic field. The sheets themselves can evolve in a complex way as they may bifurcate, or they may form rods as they pinch away from the bulk of the

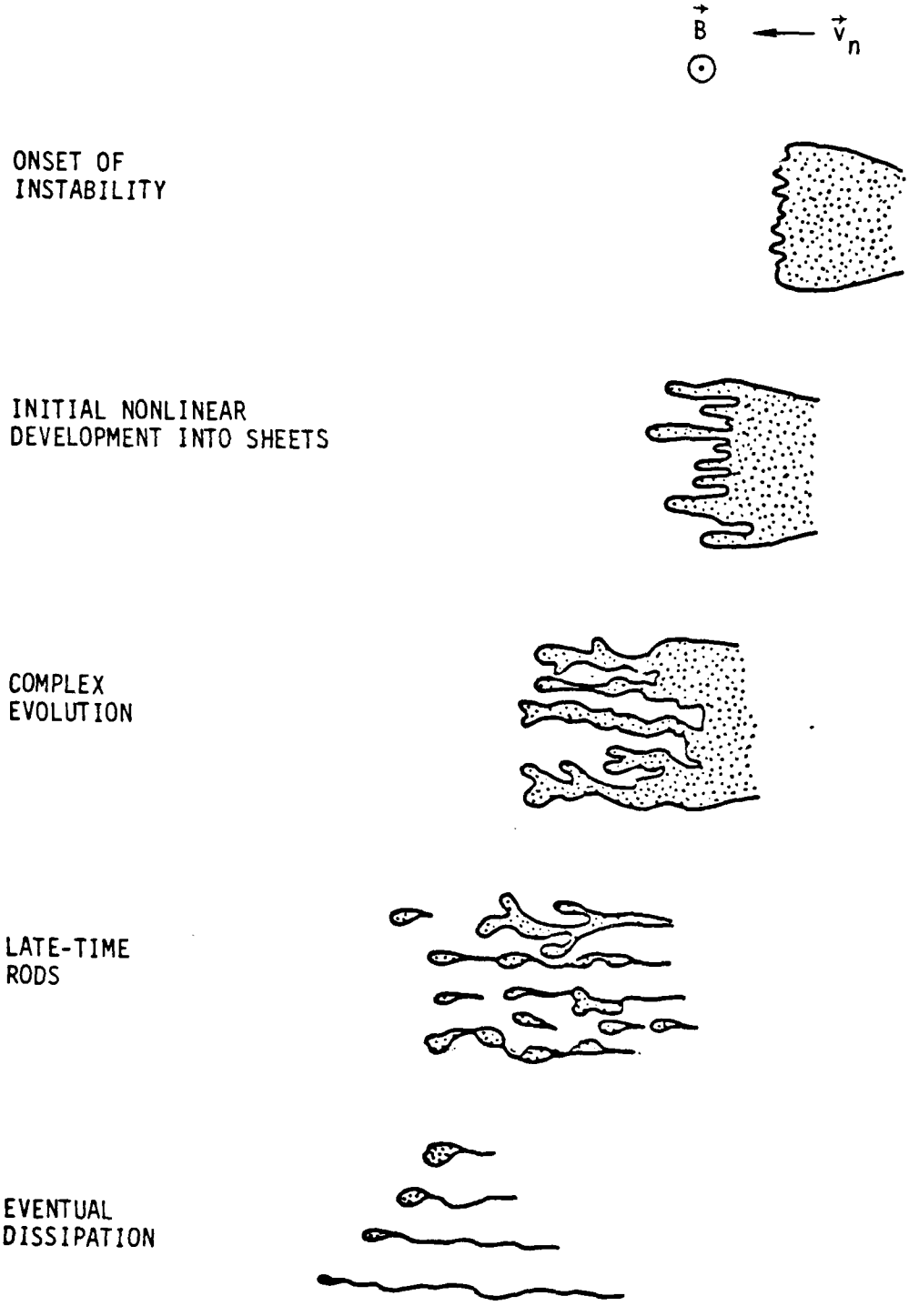

Figure 4. Qualitative evolution of striations as deduced from the observation of ionospheric barium clouds.[9]

plasma cloud. As time progresses, the number of rods increases. The rods eventually dissipate as they ablate into very thin sheets.

A successful laboratory simulation of striation evolution should also be expected to have the qualitative features illustrated in Figure 4. A major advantage of the laboratory simulation would be that appropriately placed wires could be used to affect the development of individual striations. For example, with the capability of being able to eliminate all striations but one with wire barriers, experiments could be conducted to study how the presence of neighboring striations affects the development of individual striations. Also, if wires could be used to destroy the plasma bridge between the tips of striations and the bulk plasma, then experiments should be possible clarifying the significance upon striated plasmas of attachment or disattachment to bulk plasma.

For nuclear-effects simulations like SCENARIO,[12-13] the characteristic scale sizes for striations transverse to the magnetic field are much smaller than the distance corresponding to the spacing between grid points. The striations are microscopic features for the simulations, and effects attributable to the presence of striations must be treated in a statistical manner. The striation convection algorithm in SCENARIO calculates the convection of striations in a statistical way throughout the later-time, high-altitude, nuclear environment.[12] An implicit but unproven assumption in the derivation of the algorithm is that the motion of individual striations is determined by field-line-integrated, transverse, current-density fields over scale sizes much larger than the transverse scale size of individual striations; therefore, the proximity of a single striation to its nearest neighbors is assumed to have no special significance.

In the laboratory simulation, the neutral wind can be permitted to have shear in the directions transverse to the magnetic field; therefore, the motion of fully-formed striations can be studied to determine whether they move in a manner consistent ith the direction of the neutral wind and large-scale, self-consistent, electric-field forces. Furthermore, if wire barriers can be used to eliminate some striations, it should be possible to determine the degree that proximity to neighboring striations affects striation convection.

SECTION 4
DIAGNOSTICS FOR THE LABORATORY SIMULATIONS

Plasma diagnostics, for the laboratory simulation of structured plasmas in later-time HANE plasmas, consist of a variety of miniaturized particle collecting probes to determine plasma density, electron and ion temperature, and density fluctuations. Cylindrical Langmuir probes are used to monitor plasma density and $T_{\perp,e}$, and they can also be the primary method for measuring the temporal and spatial development of plasma structures, e.g., striations during the neutral wind injection. Single-sided planar disc probes will be used to monitor $T_{\parallel,e}$. Two of the disc probes can be mounted back-to-back and monitored differentially to determine if any net current flow exists along B_0. To measure the ion temperature, T_i, a gridded, biased Faraday cup (energy analyzer) can be constructed. A schematic drawing of such an ion analyzer is given in Figure 5. Principles of operation and specific design details may, for all three of the above mentioned probes, be found throughout the plasma physics literature.[14-19]

One difficulty involved in measuring the temperature, T, for both ions and electrons is the interpretation of probe currents in a high magnetic field. For $B_0 \cong 3$ kG, the Larmor radius for the electrons will be $r_e \lesssim 10^{-3}$ cm, which is much smaller than the anticipated probe dimensions of 0.1 cm x 10^{-2} cm (radius). The electron gyrofrequency, $\omega_{ce}/2\pi \cong 10$ GHz, may also be greater than the electron plasma frequency $\omega_{pe}/2\pi \cong 1$ GHz at $n_e = 10^{10}$ cm^{-3}. Thus, the electrons can be strongly magnetized; therefore, to interpret $T_{\perp,e}$ from the cylindrical probe I-V characteristic must involve scaling the temperature obtained from a more exact, albeit more complicated method, such as using test ion acoustic waves. By monitoring the wave length at a given driving frequency greater than the ion-cyclotron frequency, the ion sound speed can be determined as $C_s \approx f\lambda$. Then, using the relation for these waves, $C_s^2 = kT_e/M_i$, and the known ion mass, a temperature may be inferred. Temperatures measured and compared using these two techniques have been shown to differ by not more than 10-15% in the present configuration with the magnetic-field strength of 50 gauss.

Absolute density measurements using Langmuir probes are subject to large errors in a magnetic field. Thus, only relative density and fluctuation measurements can be made using these probes. The absolute density can be measured by observing the cone-angle of rf resonant surfaces excited with a

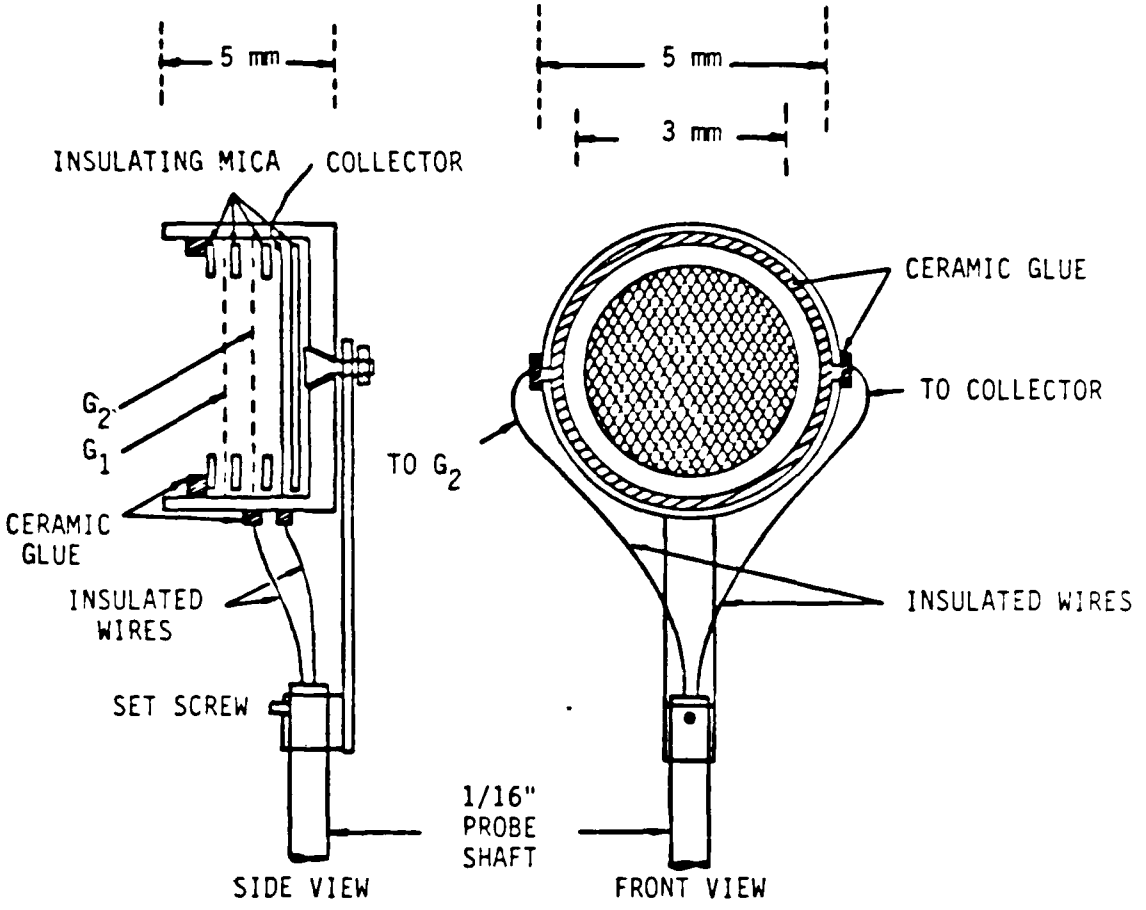

MICA THICKNESS ≈ 0.2 mm
GRID: 200 LINES/in.(STAINLESS)

Figure 5. Ion energy analyzer.

small rf probe.[19] From the cone angle Θ_c, the electron plasma frequency ω_{pe} is computed according to

$$\omega_{pe}^2 = (\omega_{ce}^2 - \omega^2) \left(\frac{\omega_{ce}^2 \sin^2 \Theta_c}{\omega^2} - 1 \right)^{-1} \tag{9}$$

knowing ω_{ce} and the rf driving frequency ω.

To determine ω_{ce}, or essentially B, diamagnetic loop probes can be used to monitor the time varying magnetic field $\partial B/\partial t$. It may also be possible to use a heat resistant Hall probe with moderate time response (10 kHz) to measure the field directly.

SECTION 5
TWO-PROBE CORRELATION STUDIES

The measurement of power-spectral densities for the scaled laboratory simulations should provide a significant basis for determining the effects of actual HANE structures on communications and tracking; therefore, we have undertaken actual experiments to demonstrate our capability to measure frequency and wave number spectrums.

For these experiments, plasma turbulence was generated by an axial electron current (parallel to B_0) which thereby excited a broad spectrum of ion acoustic and electron cyclotron waves in the background steady-state plasma. The electron drift was driven by a positive voltage pulse applied to a 15 cm diameter anode plate at one end of the plasma chamber. The pulse width was varied from 1 to 10 ms but was usually set at 4 ms. This method of generating the turbulent wave spectrum was used since it was found that the turbulence inherent in the plasma-density gradients at low magnetic field values ($B_0 \gtrsim 10$ gauss) was such that the correlation length r_c was much smaller than a typical wavelength. Thus, a more controlled means of producing the waves was used, yielding turbulent waves that were correlated to distances comparable to a wavelength.

The two probes consisted of 2 mm diameter tantalum discs ($A = 2\pi r^2 = 6.3 \times 10^{-2}$ cm^2) mounted axially and radially with respect to the main turbulent plasma column which had a diameter roughly defined by the anode plate (15 cm) and an axial extent of 40-50 cm in the region of uniform magnetic field. Both probes were mounted on precision drive mechanisms which could move in 0.5 mm ± 0.05 mm steps. The measured turbulent spectrum is shown in Figure 6, as $\delta n/n$ versus frequency f. This was swept over the frequency range of interest (10 kHz-2 MHz).

A schematic of the circuit used to make the wavelength measurements of the turbulent waves is shown in Figure 7. The probe was essentially monitoring fluctuations in the electron density associated with the ion acoustic turbulence. This was done by biasing the probe just above the plasma potential and measuring the fluctuating electron current drawn to the probe as a voltage drop across the 1 kΩ load resistor. This voltage signal was then ac coupled into a preamplifier (gain of 100) and then fed to narrow ($\Delta\omega/\omega \sim 1/35$) bandpass filters. A schematic for these "active" filters which were constructed and calibrated at JAYCOR is given in Figure 8. A plot of the

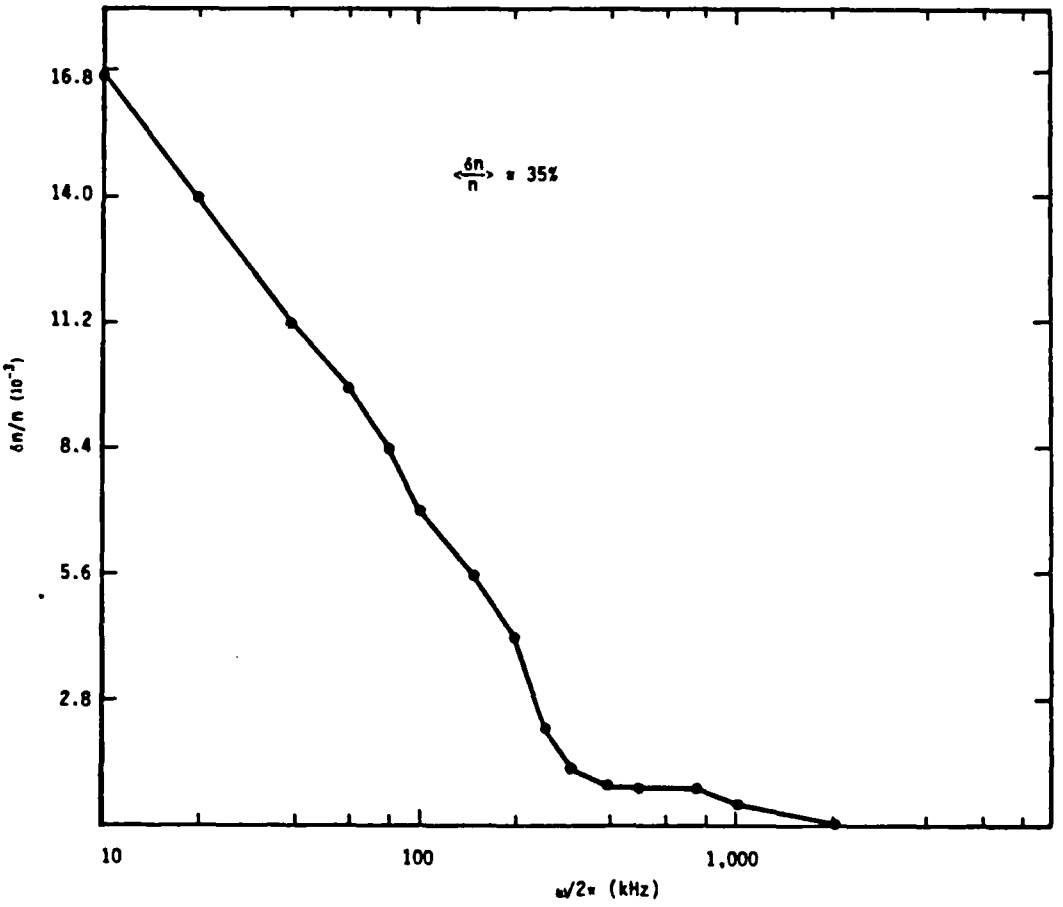

Figure 6. Measured frequency spectrum of ion acoustic turbulence. H_e plasma, $n_e = 2 \times 10^9$ cm^{-3}, $I_A = 0.20$ A.

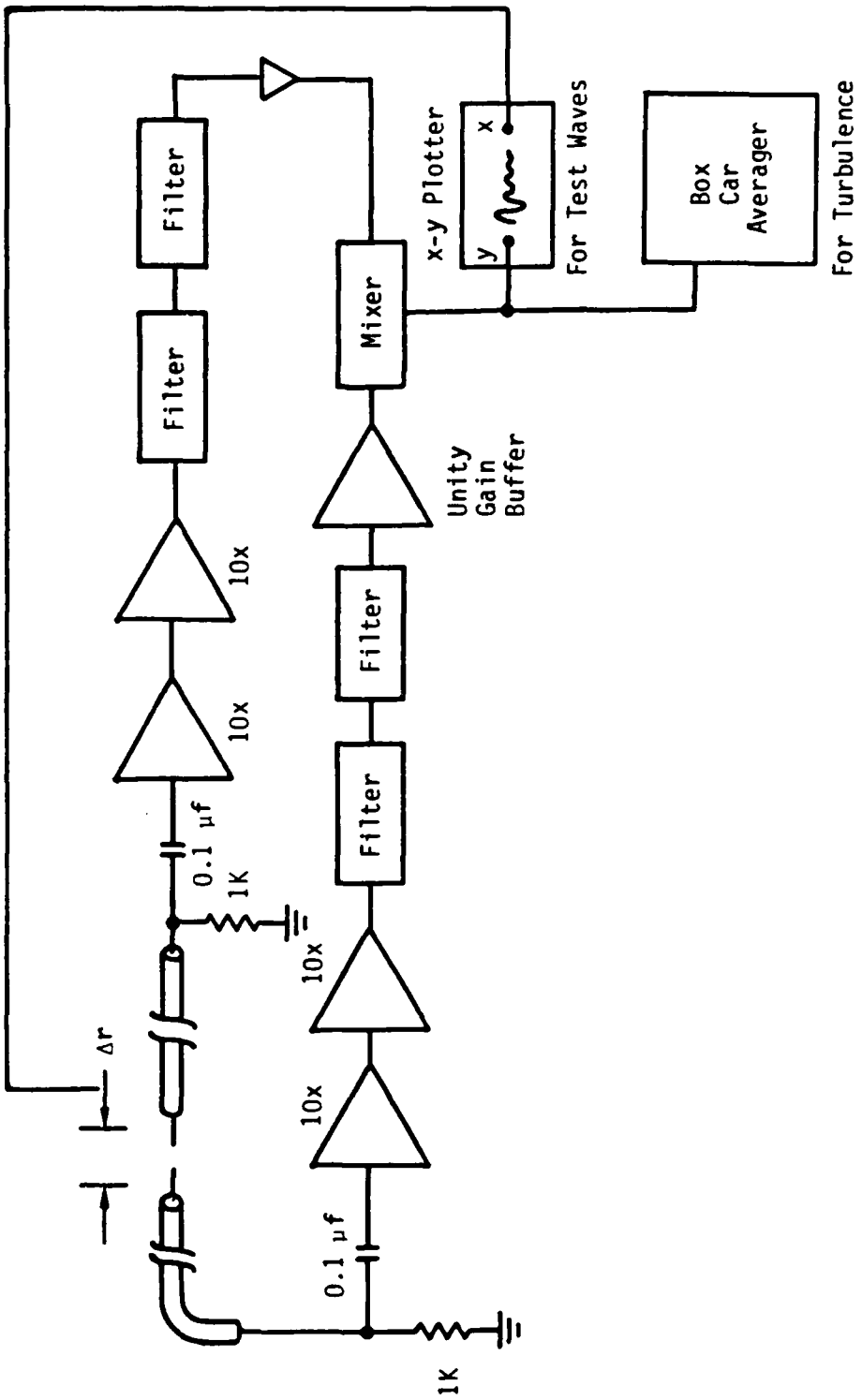

Figure 7. Schematic of the two-probe autocorrelation configuration.

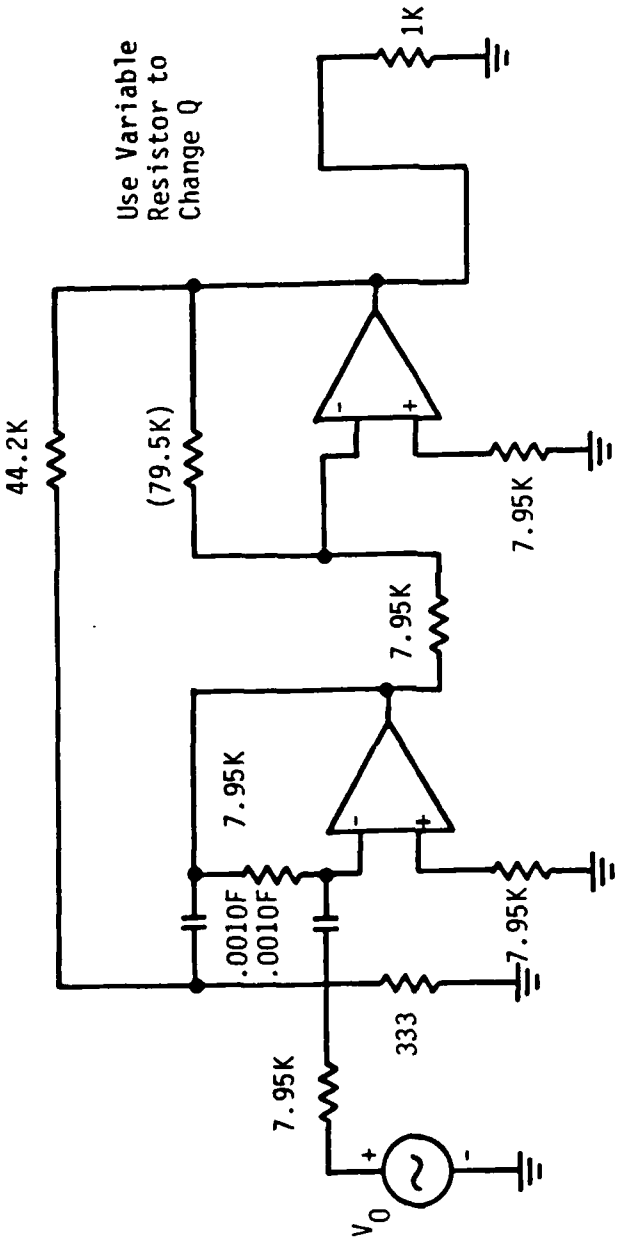

Figure 8. Burr Brown design BPF, FC = 100 KHz, Q = 25.

frequency response of a filter tuned to 93 kHz is shown in Figure 9, measured using a swept frequency network analyzer. These filters boosted the signal amplitude at the pass-band frequency an additional factor of 10 and then a unity gain buffer amplifier was used to drive the 50 Ω impedance of the mixer (signal multiplier).

The mixer output contained the sum and difference frequencies of the two probe signals, so a low-pass filter was used to suppress the 2ω portion of the signal. This low frequency signal (~dc for test waves and ~ 1 kHz for turbulent waves) was then averaged over many anode plate current pulses using a digital storage oscilloscope (Tektronix 7854). With one probe fixed, the other probe was moved and the average mixed signal value was recorded and plotted versus probe position as an interferogram to determine the wavelength of the particular frequency mode.

Small amplitude test waves were launched using the reference (fixed) probe as a check on the electronics to ascertain what wavelengths we could expect to see in the turbulent wave case. Figure 10 shows a test wave interferogram taken at a driving frequency of f = 250 kHz. There was a fairly good correlation out to $\Delta z \cong 20$ mm, and from the measured wavelength $\lambda \cong 8.5$ mm, the sound speed was calculated as $C_s = f\lambda = 2.1 \times 10^5$ cm/s. For the helium plasma which was used here, this corresponds to an electron temperature $T_e \cong 0.2$ eV since $C_s^2 = kT_e/M_i$. This was comparable to the temperature measured using a swept Langmuir probe where $T_e \cong 0.1$-0.3 eV. Figure 11 shows a similar curve taken at f = 100 kHz yielding $C_s \cong 1.9 \times 10^5$ cm/s and $T_e \cong 0.14$ eV. All test waves and turbulent wave measurements were done axially, along the magnetic field, since the waves were quickly decorrelated as one moved radially across the field. The anode plate was located at $z \cong +200$ mm.

The turbulent wave correlation data showed much stronger damping than the test wave case, probably due to the much smaller amplitude of the wave (mV versus V). An interferogram taken at 100 kHz is shown in Figure 12. The slight minimum at $\Delta z = 0$ was due to a shadow effect of the probes being so close to each other. The curve went through zero between 4 and 5 mm which was interpreted as the $\lambda/4$ distance, and then rapidly decayed to zero (no correlation). For $\lambda \cong 18$ mm, this gave $C_s = 1.8 \times 10^5$ cm/s and $T_e = 0.13$ eV. Additional scans were taken at 250, 500, 750, and 1,000 kHz with similar waveforms. The results at 1 MHz, however, were inconclusive since the interferogram decayed monotonically to zero, with no zero crossings. ($f_{pi} \cong$

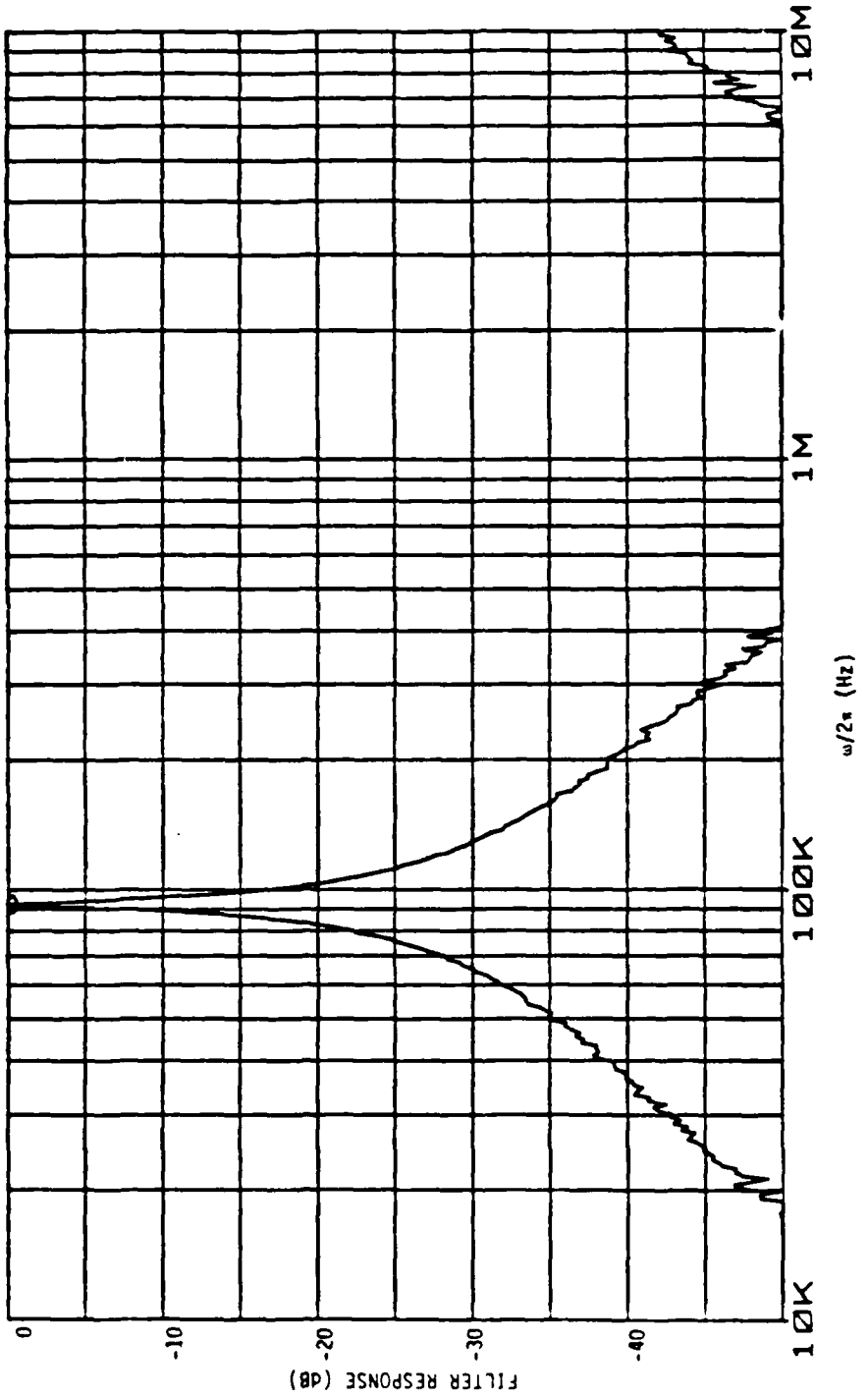

Figure 9. Active band-pass filter frequency response, filter tuned to 93 kHz; $\Delta f/f_0 = 1/35$.

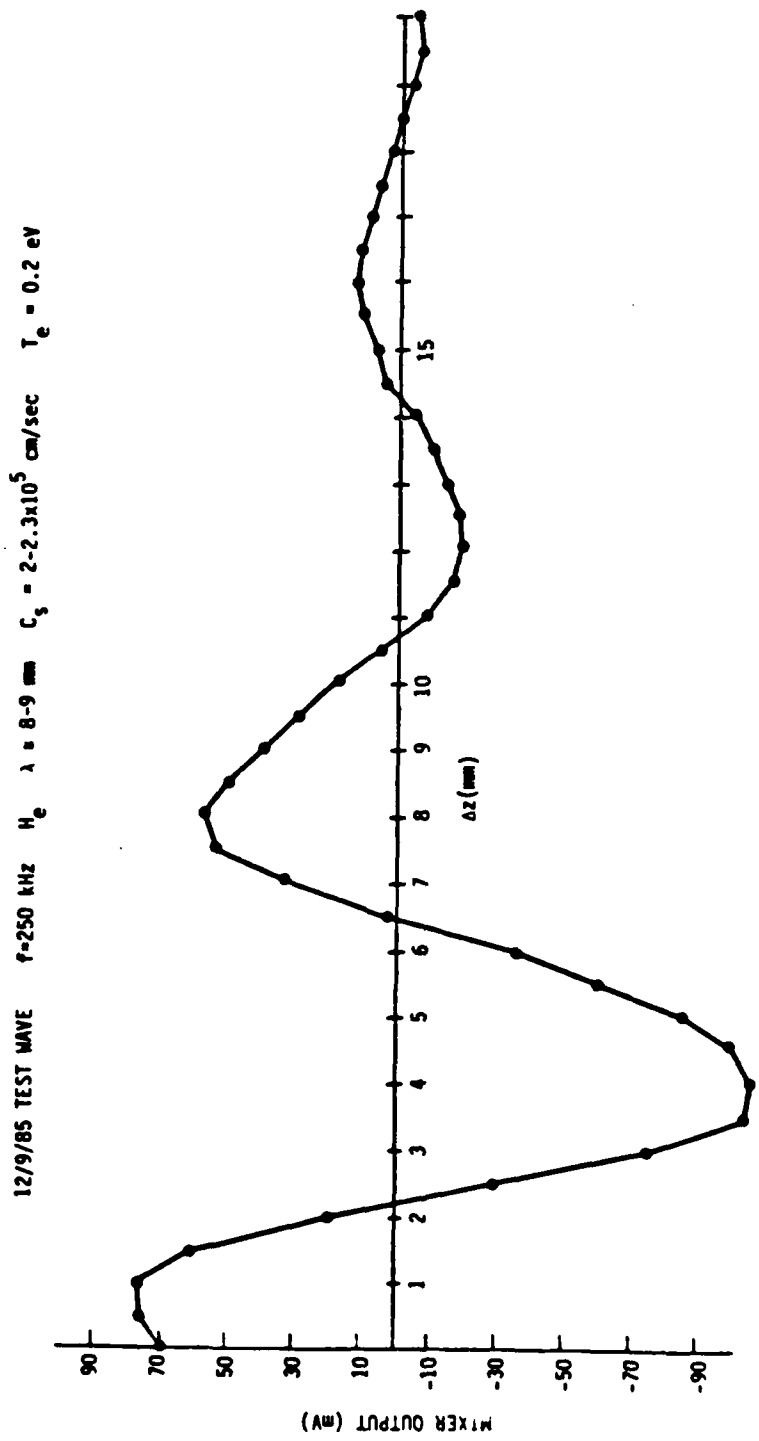

Figure 10. Test wave interferogram for helium plasma recorded at a driving frequency of 250 kHz.

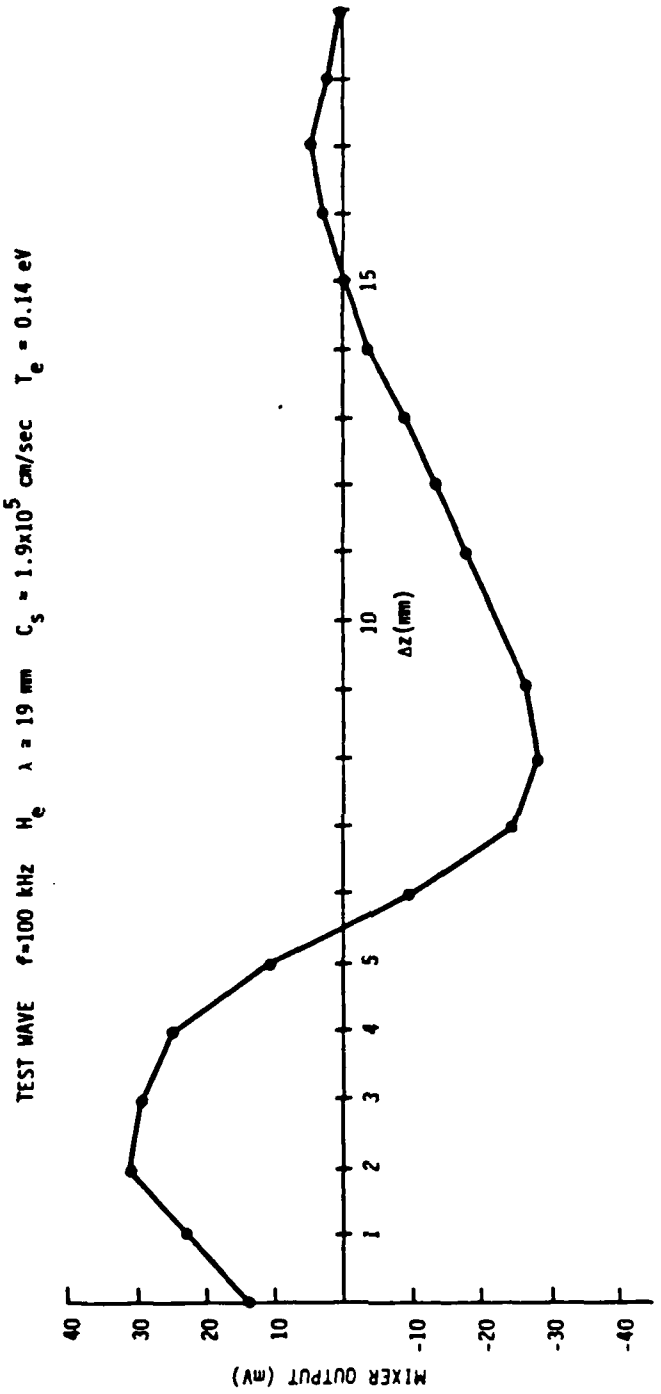

Figure 11. Test wave interferogram for helium plasma with driving frequency at 100 kHz.

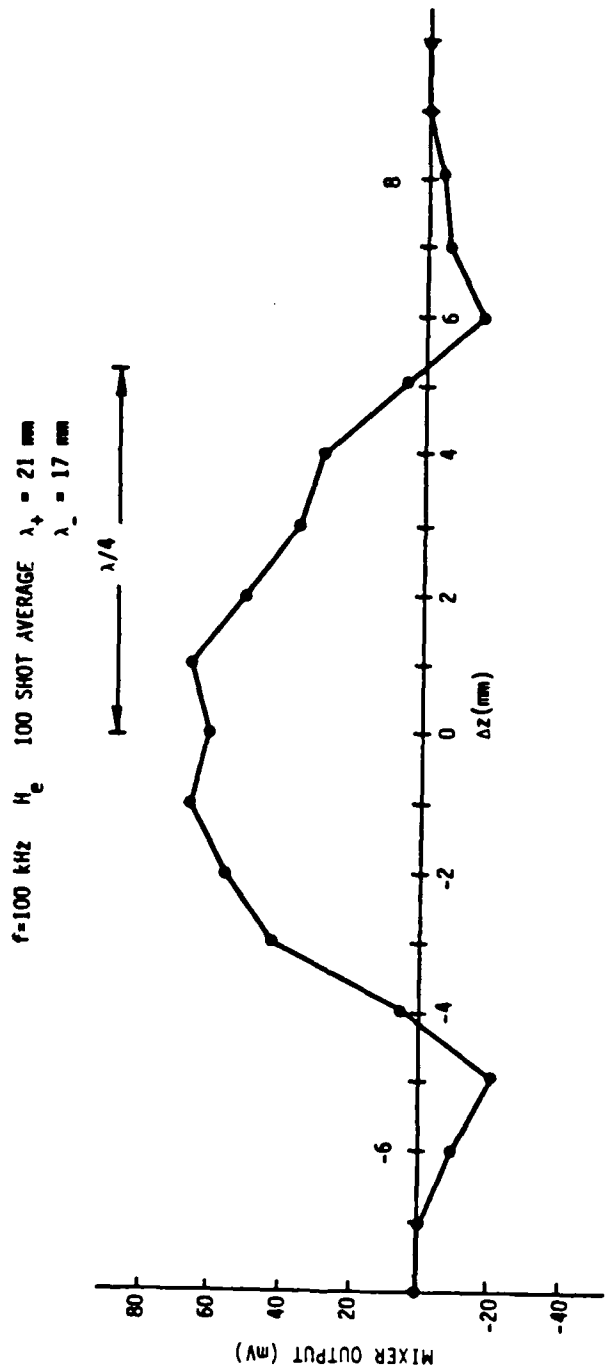

Figure 12. Wave correlation data at 100 kHz.

4 MHz at $n_e = 2 \times 10^9$ cm^{-3}). Figures 13 and 14 show interferograms at 500 and 750 kHz, respectively. The results of the 5 different frequency scans were summarized in Table 1. A plot of the measured wavelengths versus frequency was shown in Figure 15, identifying these waves as ion acoustic in nature, with an average electron temperature of $T_e \cong 0.18$ eV.

Table 1. Interferogram deduced wave number data.

f(kHz)	k	λ(mm)	C_s(x 10^5 cm/s)	T_e(eV)
100	3.49	18.0±2.0	1.8±0.2	0.13±0.03
250	8.90	7.0±1.0	1.8±0.2	0.13±0.03
500	15.70	4.0±1.0	2.0±0.5	0.16±0.08
750	20.9	3.0±0.5	2.3±0.3	0.21±0.06

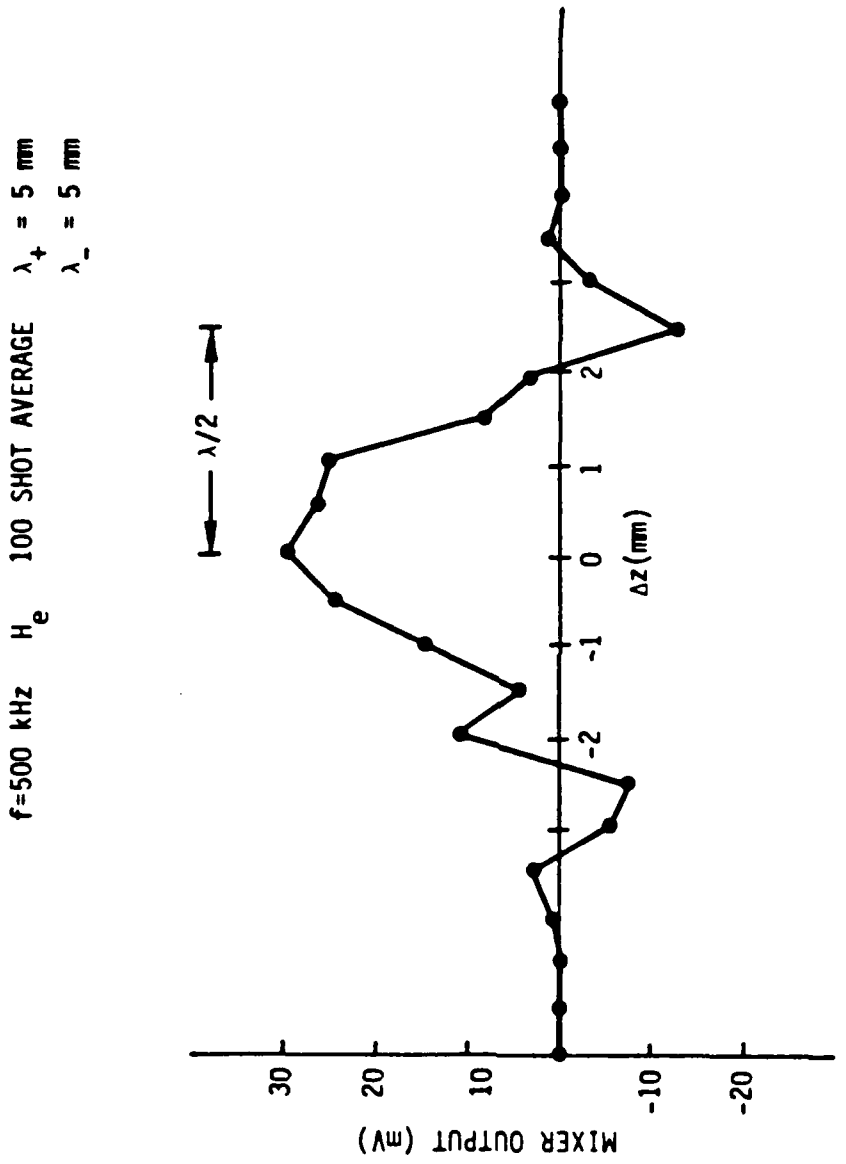

Figure 13. Interferogram wave correlation data recorded at 500 kHz.

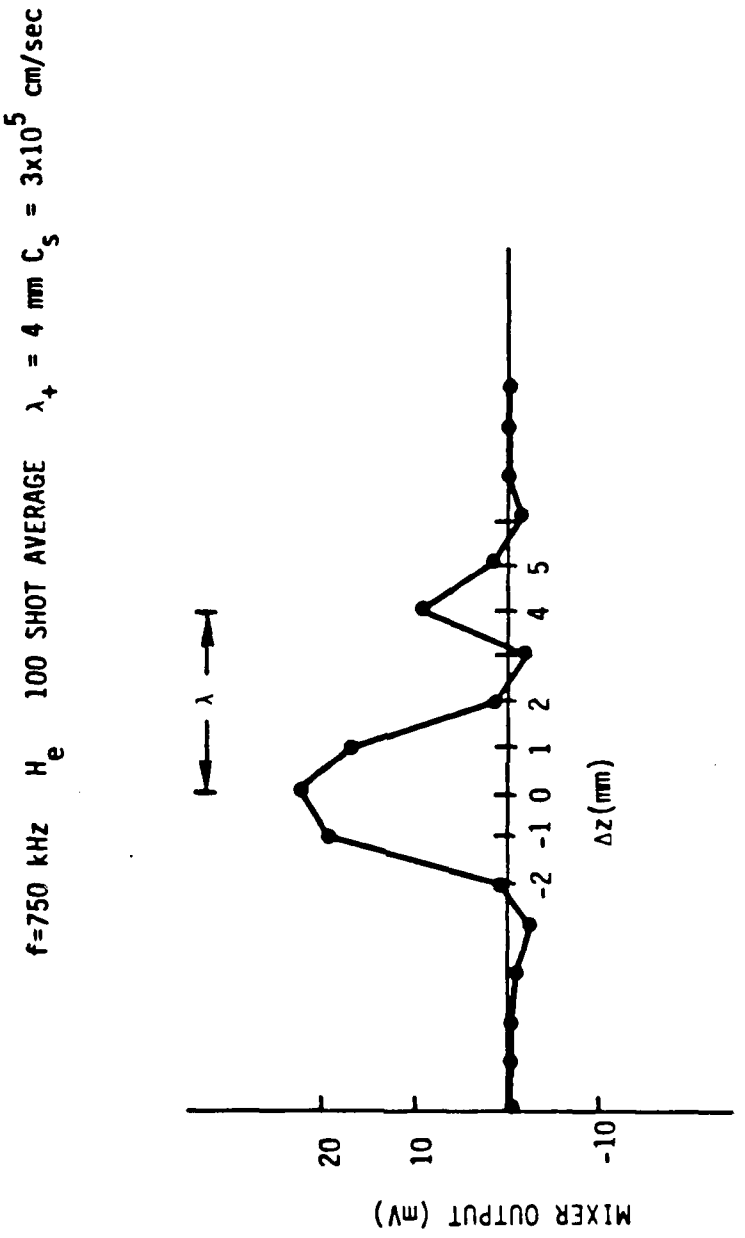

Figure 14. Interferogram wave data recorded at 750 kHz.

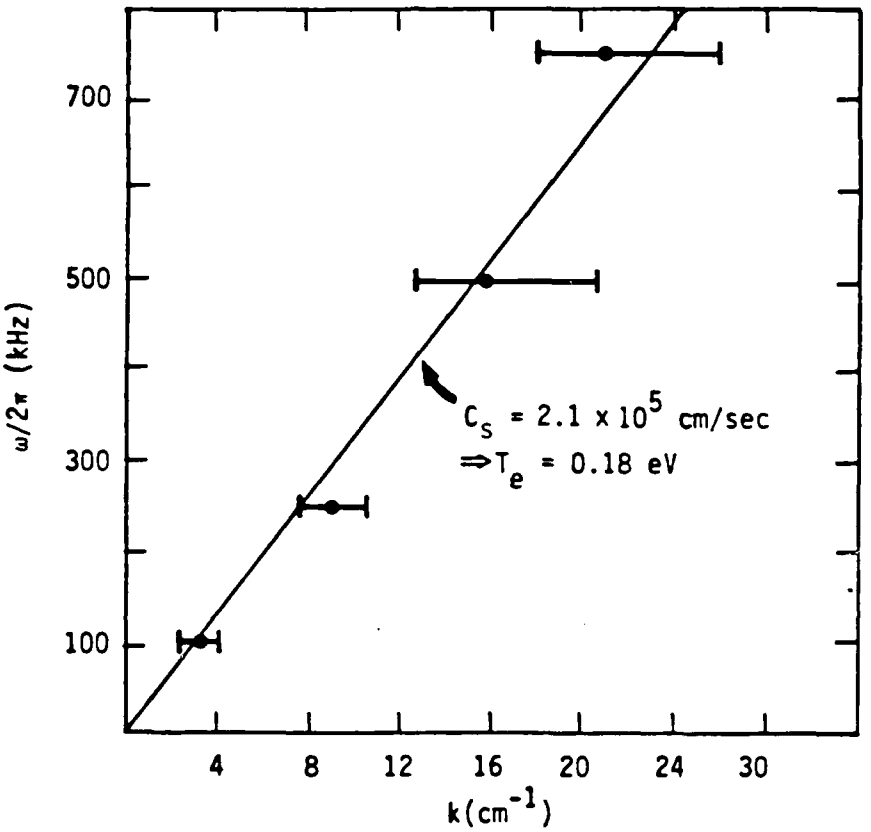

Figure 15. Wave dispersion ω versus k for frequencies and measured wavelengths. H_e plasma, $P_o \cong 1 \times 10^{-4}$ Torr, $I_A = 0.17$ A.

SECTION 6
NEUTRAL-WIND SOURCE

To undertake laboratory simulations of plasma-structure formation in the ionosphere, neutral wind velocities ~ 1 x 10^5 cm/s and neutral densities ~ (10^{12}-10^{14}) cm^{-3} are suggested by the scaling laws. The well-established technology of Laval nozzles can provide the requisite neutral winds with velocities corresponding to ~ 0.3-1 eV particle energies and neutral densities ~ 10^{11}-10^{13} cm^{-3};[20] therefore, the Laval nozzles are clearly logical and relevant for the laboratory simulations.

A Laval nozzle is an air-flow tube that is used to produce supersonic gas flows. They are used in wind tunnel experiments and they are used to supply the puffed gas on several of the gas puffed z pinch machines. Andersen et al. used a mock Laval nozzle to simulate in the laboratory supersonic expansion of a solar wind,[20] and they formed virtual boundaries on their nozzle with a magnetic field. JAYCOR currently retains the services of Will Peschel, an engineering specialist who has designed and built hundreds of Laval nozzles.

Laval nozzles can readily supply high particle densities but they are limited to high velocities (greater than 1 x 10^5 cm/s) at intermediate densities (1 x 10^{11} to 1 x 10^{13}) cm^{-3}. The nozzles cannot function below 1 x 10^{10} cm^{-3} as they must operate in a pressure regime where the mean free path of the gas molecules is much smaller than the smallest dimension of the nozzle. Gas is compressed into a Laval nozzle and reaches a Mach 1 velocity at the minimum nozzle cross-section. The emerging gas goes through a pressure discontinuity at the Mach 1 interface and expands with increasing velocities out through the exit. Mach numbers up to 10 are easily achieved. However, the gas must be in a continuum state (collisional) at the nozzle entrance. Large mean free paths inhibit uniform gas flow and acceleration. To achieve 1 x 10^4 cm/s at 1 x 10^{11} cm^{-3} on the downstream side means that we would have to use supercooled gases (lower speed of sound) and high Mach numbers in excess of 10 (large area ratios for continuum gas flow). It is possible to achieve 1 x 10^4 to 2 x 10^5 cm/s at 1 x 10^{14} cm^{-3}.

Figure 16 shows a schematic of a possible laboratory neutral wind source. Moving from left to right across the figure we have a cooled neutral gas reservoir, a Varian piezoelectric puff gas valve, a flow quieting section,

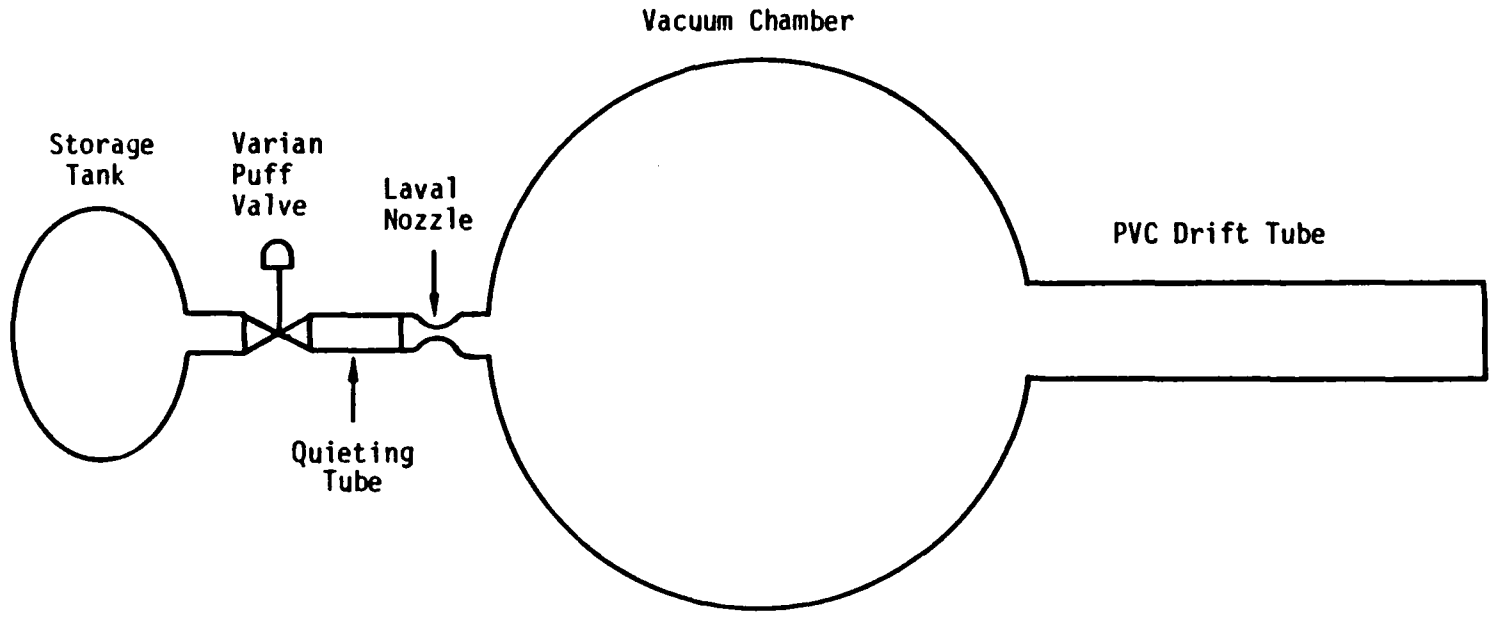

Figure 16. Schematic of neutral wind assembly.

a two-dimensional Laval nozzle, our plasma vacuum chamber, and an extension drift tube.

The following specifications would be used to build a nozzle capable of delivering ~ 1 x 10^4 to ~ 2 x 10^5 cm/s neutral wind at 10^{-3} torr, with a uniform two-dimensional cross-section 2 x 10 cm without flooding the vacuum chamber. The critical parts of the nozzle configuration consist of throat size to molecular mean free path and total gas injected compared with chamber pressure. A gas moving at 1 x 10^5 cm/s will take 10^{-3} s to "bounce" off the walls of our chamber. The gas fills a 2 cm x 10 cm x 100 cm volume at 10^{-3} torr. The flow rate equals the pressure divided by time and multiplied by the volume. The flow rate can also be defined in terms of the nozzle.

$$\omega = \frac{p \times V}{t} = \frac{K \times A^* \times P_o}{\sqrt{T_o}} \tag{10}$$

where ω is the flow rate, p is the neutral gas pressure, V is the gas volume in cm^3, t is its on time, K is a conversion constant = 3.4, A* is the nozzle throat area in cm^2, P_o is the stagnation pressure in torr, and T_o is the stagnation temperature (determined from nozzle specification in Rankines). There are no unknowns. Nozzle design tables dictate the throat area and stagnation values.[21]

From nozzle design tables, A/A* (exit area/throat area) equals 4.35 for a Mach 3 nozzle. P/P_o (delivered pressure/stagnation pressure) = 2.7 x 10^{-2}. Similarly, T/T_o = 0.36. The speed of sound is $a = k' \sqrt{T}$, a = 3 x 10^4 cm/s ÷ (Mach 3). k' ≈ 50 for T in Rankines.

$$\begin{aligned} P_o &= 10^{-3}/2.7 \times 10^{-2} = 0.04 \text{ torr} \\ T_o &= a^2/49 = 500°R \ (40°F) \\ A^* &= 20/4.35 = 4.6 \ cm^2 \quad . \end{aligned} \tag{11}$$

Thus, we have the reservoir pressure and can infer that the molecule mean free path is small compared to the throat diameter. The gas is maintained close to room temperature (desired), and the reservoir pressure and nozzle dimensions are readily achieveable.

How can we verify the neutral wind output? That part is easier to solve. We can use ionization gauge elements to detect the fast gas flow and quantify the neutral density. An ionization gauge works by ionizing a known fraction of the surrounding neutral gas population and accelerates the just formed ions into a collector. The gauges contain electron emitting filaments that ionize the neutrals with 60 eV electron energies. The gauges can respond to microsecond changes in pressure. Their response is linear with pressure as long as the ion sheath that forms around the sensing element is not space-charge limited. They are sometimes called Residual Pressure Analyzers (RPA).

A single gauge element cannot differentiate between directed gas flow and net pressure increase because it measures the product of density times velocity. We would use two gauges to monitor gas velocity via a time-of-flight measurement. We would separate the two detectors by at least 2 cm (at 1×10^5 cm/s that means a 20 microsecond transit) to insure nonperturbing sheath current measurements.

SECTION 7
CONCLUSIONS

Scaling laws have been derived for relating the evolution of plasma structures in the later-time HANE environment with the large plasma chamber at JAYCOR. In the derivations it is argued that the proper scaling of the ion-gyroradius is extremely important; therefore, to assure reasonable magnetic-field strengths in the laboratory, we suggest that a fill gas with very low atomic mass (i.e., hydrogen) may be advantageously used in individual laboratory simulations.

The initial plasma configuration and possible laboratory studies are described. For the cylindrical tank at JAYCOR a cylindrical density profile, with the electron density greater at smaller radii than at larger radii, is desirable and experimentally reasonable. The externally applied magnetic field is directed axially, and the externally-applied neutral wind is directed across the cylindrical plasma. This laboratory configuration permits simulations for elucidating the role of parallel plasma currents and perpendicular plasma processes on the formation of striations. Experiments can also be conducted for determining the evolutionary characteristics of single striations and aggregates of striations. The extensive use of probes to measure plasma parameters and power-spectral densities can assure the relevance of the laboratory simulations to the understanding of plasma structures in later-time HANE plasmas. The well-established technology of Laval nozzles can be used to drive a neutral wind across the cylindrical laboratory plasma.

SECTION 8
LIST OF REFERENCES

1. Sperling, J. L., The Scaling of Some Processes Affecting Structure in the High-Altitude Nuclear Environment, JAYCOR Rep. J530-83-102, JAYCOR, San Diego, California (1983).
2. Sperling, J. L., and A. J. Glassman, Short-Circuiting, Ion-Viscous, and Ion-Inertial Effects in Striation "Freezing", J. Geophys. Res. 90, 8507 (1985).
3. Sperling, J. L., Progress Report for the Period September 16 to November 15, 1985 under Contract No. DNA001-85-C-0063, JAYCOR Rep. J530-85-339/2427 (1985).
4. Longmire, C. L., A Study of the Feasibility of Using Laser Exploded Plasmas to Simulate High Altitude Nuclear Explosions, draft prepared for the Defense Nuclear Agency by Los Alamos National Laboratory and Mission Research Corporation, Section 2 (1981).
5. Sperling, J. L., and A. J. Glassman, J. Geophys. Res. 88, 10091 (1983).
6. Sperling, J. L., and A. J. Glassman, J. Geophys. Res., 90, 2819 (1985).
7. Sperling, J. L., J. Geophys. Res. 89, 6793 (1984).
8. Sperling, J. L., and A. J. Glassman, The Role of Finite Parallel Conductivity and Other Classical Processes on the Evolution of High-Altitude Plasmas, Rep. DNA-TR-84-196, Defense Nuclear Agency, Washington, D.C. (1984).
9. Linson, L. M., and G. Meltz, Theory of Ion Cloud Dynamics and Morphology, Analysis of Barium Clouds, Rep. RADC-TR-72-736, Vol. 1, Ch. 5, Avco Everett Res. Lab., Everett, Mass. (1972).
10. Prettie, C. W., U-Shaped Curve Constant Determined by Barium Release Measurements, Rep. PD-BRA-84-320R, Berkeley Res. Ass., Berkeley, CA (1984).
11. Prettie, C. W., S. Y. F. Chu, and J. B. Workman, Gradient-Drift Instability of a Diffusive Equilibrium, Rep. BRA-85-304R, Berkeley Res. Ass., Berkeley, CA (1985).
12. Stagat, R. W., D. S. Sappenfield, and J. P. Incerti, The SCENARIO Code: Modifications in Version II and the Striation Convection Theory, Rep. AFWL-TR-80-124, Air Force Weapons Laboratory (NTYC), Kirtland Air Force Base, NM (1982).

13. Prettie, C. W., S. Y. F. Chu, and J. B. Workman, The Microstructure Theory for Three Dimensional Plasma Transport, Rep. DNA-TR-81-270, Defense Nuclear Agency, Washington, D.C. (1983).
14. Taylor R., H. Ikezi, and D. Baker, Phys. Rev. Lett. 24, 206 (1970).
15. Chen, F. F., "Electric Probes," in Plasma Diagnostic Techniques, ed. by Huddlestone & Leonard (Academic Press, 1965).
16. Shott, L., Plasma Physics, ed. by W. Lochte-Holtgreven, Ch. 11 (North Holland, 1968).
17. Gekelman, W., and R. L. Stenzel, Phys. Fluids 21, 2014 (1978).
18. Ilic, D. B., Phys. Fluids 20, 1717 (1977).
19. Fisher, A. K., and R. W. Gould, Phys. Fluids 14, 857 (1971).
20. Andersen, S. A., et al., Phys. Fluids 12, 557 (1969).
21. Liepmann, H. W., and A. Roshko, Elements of Gas Dynamics, p. 417 (John Wiley and Sons, 1957).

DISTRIBUTION LIST

DEPARTMENT OF DEFENSE

DEFENSE INTELLIGENCE AGENCY
ATTN: RTS-2B

DEFENSE NUCLEAR AGENCY
ATTN: NATF
ATTN: NAWE
3 CYS ATTN: RAAE
ATTN: RAAE K SCHWARTZ
ATTN: RAAE P LUNN
ATTN: RAAE T WALSH
ATTN: RAEE
ATTN: STNA
4 CYS ATTN: STTI-CA

DEFENSE TECHNICAL INFORMATION CENTER
12 CYS ATTN: DD

FIELD COMMAND/DNA DET 2
LAWRENCE LIVERMORE NATIONAL LAB
ATTN: FC-1

DEPARTMENT OF THE NAVY

NAVAL RESEARCH LABORATORY
ATTN: CODE 4180 J GOODMAN
ATTN: CODE 4700 S OSSAKOW
ATTN: CODE 4720 J DAVIS
ATTN: CODE 4750 P RODRIGUEZ

DEPARTMENT OF THE AIR FORCE

AIR FORCE GEOPHYSICS LABORATORY
ATTN: CA/A STAIR
ATTN: LID/J RAMUSSEN
ATTN: LIS/J BUCHAU
ATTN: LS
ATTN: LS/R O'NIEL
ATTN: LSI/H GARDINER
ATTN: LYD/K CHAMPION

AIR FORCE WEAPONS LABORATORY, AFSC
ATTN: NTN
ATTN: SUL

DEPARTMENT OF ENERGY

LOS ALAMOS NATIONAL LABORATORY
ATTN: D SAPPENFIELD
ATTN: D SIMONS
ATTN: J WOLCOTT
ATTN: MS J ZINN
ATTN: R JEFFRIES
ATTN: T KUNKLE, ESS-5

SANDIA NATIONAL LABORATORIES
ATTN: A D THORNBROUGH
ATTN: D DAHLGREN
ATTN: ORG 1231 T P WRIGHT
ATTN: ORG 314 W D BROWN
ATTN: ORG 332 R C BACKSTROM
ATTN: SPACE PROJECT DIV
ATTN: TECH LIB 3141

DEPARTMENT OF DEFENSE CONTRACTORS

AUSTIN RESEARCH ASSOCIATES
ATTN: J THOMPSON

BERKELEY RSCH ASSOCIATES, INC
ATTN: C PRETTIE
ATTN: J WORKMAN
ATTN: S BRECHT

EOS TECHNOLOGIES, INC
ATTN: B GABBARD
ATTN: W LELEVIER

JAYCOR
2 CYS ATTN: J SPERLING
2 CYS ATTN: N WILD
2 CYS ATTN: P COAKLEY

KAMAN TEMPO
ATTN: B GAMBILL
ATTN: DASIAC
ATTN: W MCNAMARA

KAMAN TEMPO
ATTN: DASIAC

M I T LINCOLN LAB
ATTN: D TOWLE
ATTN: I KUPIEC

MAXIM TECHNOLOGIES, INC
ATTN: J LEHMAN
ATTN: J MARSHALL
ATTN: R MORGANSTERN

DEPT OF DEFENSE CONTRACTORS (CONTINUED)

MISSION RESEARCH CORP
ATTN: C LAUER
ATTN: D ARCHER
ATTN: D KNEPP
ATTN: F FAJEN
ATTN: F GUIGLIANO
ATTN: G MCCARTOR
ATTN: R BIGONI
ATTN: R BOGUSCH
ATTN: R DANA
ATTN: R HENDRICK
ATTN: R KILB
ATTN: S GUTSCHE
ATTN: TECH LIBRARY

PACIFIC-SIERRA RESEARCH CORP
ATTN: H BRODE, CHAIRMAN SAGE

PHYSICAL RESEARCH, INC
ATTN: R DELIBERIS
ATTN: T STEPHENS

PHYSICAL RESEARCH, INC
ATTN: J DEVORE
ATTN: J THOMPSON
ATTN: W SCHLUETER

R & D ASSOCIATES
ATTN: B LAMB
ATTN: B MOLLER
ATTN: C GREIFINGER
ATTN: F GILMORE
ATTN: H ORY
ATTN: M GANTSWEG
ATTN: M GROVER
ATTN: R TURCO
ATTN: W KARZAS

SRI INTERNATIONAL
ATTN: C RINO
ATTN: D MCDANIEL
ATTN: D NIELSON
ATTN: G PRICE
ATTN: G SMITH
ATTN: J VICKREY
ATTN: R LEADABRAND
ATTN: R LIVINGSTON
ATTN: R TSUNODA
ATTN: W CHESNUT
ATTN: W JAYE

TOYON RESEARCH CORP
ATTN: J GARBARINO
ATTN: J ISE

VISIDYNE, INC
ATTN: J CARPENTER

END

DTIC

9-86